Side Chain Dynamics in Poly(ethyl acrylate) Studied by Molecular Dynamics Simulation

Hiroaki Kikuchi,*,# Kazuhiko Seki,† Satoru Kuwajima,†† and Norimasa Okui

Department of Organic and Polymeric Materials, Tokyo Institute of Technology, 2-12-1 Ookayama, Meguro-ku, Tokyo 152-8552

†Engineering Research Department, NOK Corporation, 25 Wadai, Tsukuba, Ibaraki 300-4247

††Nano-Simulation Associates, 825-1 Amado-cho, Villa DE201, Hanamigawa-ku, Chiba 262-0043

(Received November 6, 1998)

A molecular dynamics (MD) trajectory of 1.0 ns duration has been computed for a methyl-terminated atactic poly(ethyl acrylate) using force field parameters which we determined by ab initio molecular-orbital calculations for small molecules (RHF/6-31G level). Local side chain motions were clarified by analyses of the MD trajectory. The torsional angle autocorrelation functions (TACF) were calculated for each dihedral angle in the side chain. All of the TACF were strongly non-exponential. The entire side chain rotation was an asymmetric 180° jump motion with a rapid torsional oscillation within stable and metastable conformations, while ethyl group motion around the O(non-carbonyl)–CH_2 bond in the side chain was characterized by rapid torsional motion in the angle range from 60 to 300° involving an obscure three-site jump motion.

Atomistic computer simulations of amorphous polymers have been gathering momentum in recent years.[1—29] The purpose of these studies is to elucidate the bulk properties, including structure,[2—7] elasticity,[6—8] glass transition,[2,9—13] gas transport,[14—20] interface structure,[21] stress-strain behavior,[22—24] chain dynamics,[25—28] and dielectric relaxation.[29] Molecular dynamics (MD) simulations are especially suitable for directly observing the features of local molecular motion. Molecular dynamics simulations were employed to study the side chain dynamics of poly(ethyl acrylate) (PEA). PEA was chosen because it is industrially important as an oil-resistant material.

The purpose here is to discuss the molecular motion responsible for the mechanical properties. To this end, the side chain motion for PEA was analyzed using the MD trajectory. Generally, the side chain dynamics in the bulk state has been studied by the following techniques: NMR relaxation,[1] broad-line NMR,[30] dielectric relaxation,[31] and both inelastic and quasi-elastic neutron scattering.[32] However, extracting only the side chain motion is difficult, since the main chain motion often superimposes on the side chain motion. Moreover, polymers probed by spectroscopic measurements have been rather limited, especially the cases when the polymer structure is not simple. Our purpose in employing the MD simulation techniques is to get some information that is not available from spectroscopic experiments. If the time scale of the side chain motion is compatible with the MD time scale, the motional mode in the side chain can be easily analyzed by a statistical method, because the output from MD runs was obtained as atomic coordinate data. Such detailed information can not be obtained from experiments.

Our attention will be focused on the side chain dynamics in this paper. The quality of the sample is also examined by comparing the calculated density and thermal expansion coefficient with the experimental data. We discuss the motional mode and rate in the side chain by extraction of the elemental motion.

Models and Simulations

Computational Details: MD computations were performed with a program named GEMS/MD,[33] which is basically a collection of known MD techniques. The equations of motion numerically integrated are those of rigid-bodies rather than particles. The constant-temperature MD method is that of Nose.[34] The constant-pressure MD method is an intermediate of Andersen's method[35] and Parrinello and Rahman's one;[36] i.e., the shape of a periodic cell is restricted to be orthorhombic, but the three edge lengths are allowed to vary independently.[37] Molecule-based virials are used to calculate the pressure.[38] The scaling of coordinates associated with the change of the cell size is applied only to molecular center-of-mass coordinates.[38] Note that there is only one molecular center-of-mass in the present case.

A time increment of 1 fs was used in a numerical integration of the equations of motion. The van der Waals interactions were truncated at 7.5 Å, with truncation corrections by means of a simplified version of Williams's treatment.[39] The electrostatic forces were computed using a method called spherical Ewald truncation by Linse and Andersen,[40] with

On leave from Engineering Research Department, NOK Corporation, 25 Wadai, Tsukuba, Ibaraki, 300-4247, Japan.

a truncation radius of 7.5 Å and the Ewald parameter η (or G) = 0.3 Å^{-1}. The atoms of the PEA chain were divided into rigid-body entities in order to reduce the vibrational frequencies that limit the time increment of the integration. The rigid-body grouping is shown in Fig. 1.

Force-field parameters used in the MD simulation are shown in Table 1. The bonding parameters, i.e., parameters of the bond stretch, bending, inversion, and torsion were fitted to ab initio molecular-orbital potential surfaces of small molecules (RHF/6-31G level). For the van der Waals parameters, the method of Jorgensen et al. in the development of the OPLS force fields[41] was used; i.e., the parameters were determined so that the experimental density and cohesive energy (or heat of vaporization[41]) of small-molecule liquids, ethane through acetone in the present case (Table 2) was reproduced. Note that the MD results of methyl and ethyl acetates do not involve parameter fitting. The partial charges were determined mainly by fitting to the experimental dipole moments of isolated molecules. It is worth stressing that the properties of polymers were not used at all in the parametrization.

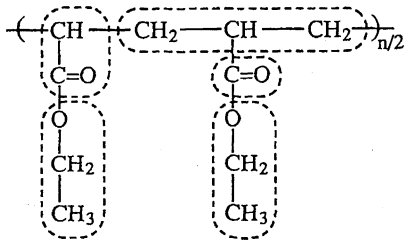

Fig. 1. Grouping of PEA atoms into rigid-body moieties.

Sample Preparation: The simulated polymer is atactic PEA with polymerization degree of 300 and molecular weight of 30065, which included methyl groups attached to chain ends. The computational sample is identical to the sample in Ref. 1. We used the united-atom model, i.e., exclusion of H atoms from explicit handling, and the PEA chain had 2102 nonhydrogen atoms. Figure 2 illustrates the essence of the sample preparation: (a) is the PEA structure in the gas-phase and (b) is a typical snapshot of condensed structures that are obtained by compression of the structure (a). The boxes drawn in the figures indicate periodic cells associated

Table 1. Force-Field Parameters of PEA[a]

Bond stretch[b]	r_0/Å	k_r/kcal mol^{-1} Å^{-2}	Bending[c]	q_0/°	k_q/kcal mol^{-1} rad^{-2}
C1–C2′	1.531	328	C–C2–C	113.3	89.5
C1–C2″	1.511	357	C–C3–C	111.0	80.0
C1–C3	1.535	354	C1–C2–O2	106.7	101.1
C2–C3	1.540	312	C3–CD–O2	112.1	74.5
C3–CD	1.506	342	C3–CD–OD	125.7	63.3
C2–O2	1.455	320	O2–CD–OD	122.2	126.5
CD–O2	1.348	471	C2–O2–CD	119.8	84.8
CD–OD	1.213	968			

Inversion[d]	K_1/kcal mol^{-1} rad^{-1}	K_2/kcal mol^{-1} rad^{-2}	K_8/kcal mol^{-1} rad^{-8}
C3	0.0	34.5	4.2×10^4
CD	−60.0	30.0	0.0

Torsion[e]/kcal mol^{-1}	V_1	V_2	V_3	V_4
C–C2–C3–C	1.27	0.58	1.06	0.0
C–C3–CD–O2	0.31	0.21	0.51	0.0
C–C3–CD–OD	−0.19	−0.08	0.25	0.0
C3–CD–O2 –C2	4.76	−1.21	0.16	0.0
OD –CD –O2 –C2	0.0	−2.69	−0.21	0.0
C1–C2–O2–CD	−1.12	−0.76	0.04	−0.18

van der Waals[f]	A/kcal mol^{-1}Å^{-12}	C/kcal mol^{-1}Å^{-6}	Partial charge/ |e|	
C1–C1	7.1×10^6	2400	OD	−0.37
C2–C2	7.1×10^6	1650	O2	−0.31
C3–C3	7.1×10^6	750	CD	0.31
CD–CD	2.9×10^6	700	C3	0.11
O2–O2	2.05×10^5	480	C2″	0.26
OD–OD	2.05×10^5	540	C1, C2′	0.0

a) The united-atom model is used. Atom types are denoted as follows. C1: CH_3 carbon. C2: CH_2 carbon in general. C2′: CH_2 carbon in the main chain. C2″: CH_2 carbon in the side chain. C3: CH carbon. CD: carbonyl carbon. O2: non-carbonyl oxygen. OD: carbonyl oxygen. C: carbon atom in general. b) $U = k_r(r - r_0)^2$. c) $U = k_\theta(\theta - \theta_0)^2$. d) This is a special term. The variable of the potential, Θ, is the sum of the 3 bond angles that are formed around the C3 and CD type atoms. The potential energy U is given by $U = K_1(\Theta - \Theta_0) + K_2(\Theta - \Theta_0)^2 + K_8(\Theta - \Theta_0)^8$, where Θ_0 is the sum of the corresponding 3 equilibrium angles. e) $U = V_1\cos\phi + V_2\cos 2\phi + V_3\cos 3\phi + V_4\cos 4\phi$. f) $U = Ar^{-12} - Cr^{-6}$. The combining rules are $A_{ij} = ((A_{ii}^{1/13} + A_{jj}^{1/13})/2)^{13}$ and $C_{ij} = (C_{ii}C_{jj})^{1/2}$. Note that nonbonding interactions between atoms separated by less than 4 bonds are excluded.

Table 2. Densities and Cohesive Energy Densities[a)]

Compound	Temp/K	Density/g cm^{-3}		Cohesive energy density/cal cm^{-3}	
		Calcd	Expt	Expt	Calcd
PEA	293.15	1.09	1.119[b)]	55	88[c)]
Reference liquids					
Ethane	184.52	0.539	0.546[d)]	55.4	57.3[d)]
Propane	231.08	0.582	0.581[d)]	52.9	53.1[d)]
Isobutane	261.45	0.606	0.595[e)]	47.4	47.2[e)]
Dimethyl ether	248.35	0.735	0.736[f)]	74.8	74.2[g)]
Acetone	298.15	0.792	0.784[h)]	93.8	91.9[i)]
Methyl acetate	298.15	0.934	0.928[j)]	97.9	89.3[k)]
Ethyl acetate	298.15	0.903	0.895[j)]	87.1	80.5[k)]

a) The cohesive energy density is defined as the energy of vaporization (ΔE_v) per volume. The calculated value of the polymer is obtained by the usual method (see Ref. 5). The experimental ΔE_v for the reference liquids are estimated from the heat of vaporization (ΔH_v) by $\Delta E_v = \Delta H_v - RT$. b) From Ref. 42. c) From Ref. 43 (swelling measurement). d) From Ref. 44. e) From Ref. 45. f) From Ref. 46. g) From Ref. 47. h) From Ref. 48. i) From Ref. 49. j) From Ref. 50. k) From Ref. 51. l) 1 cal = 4.184 J.

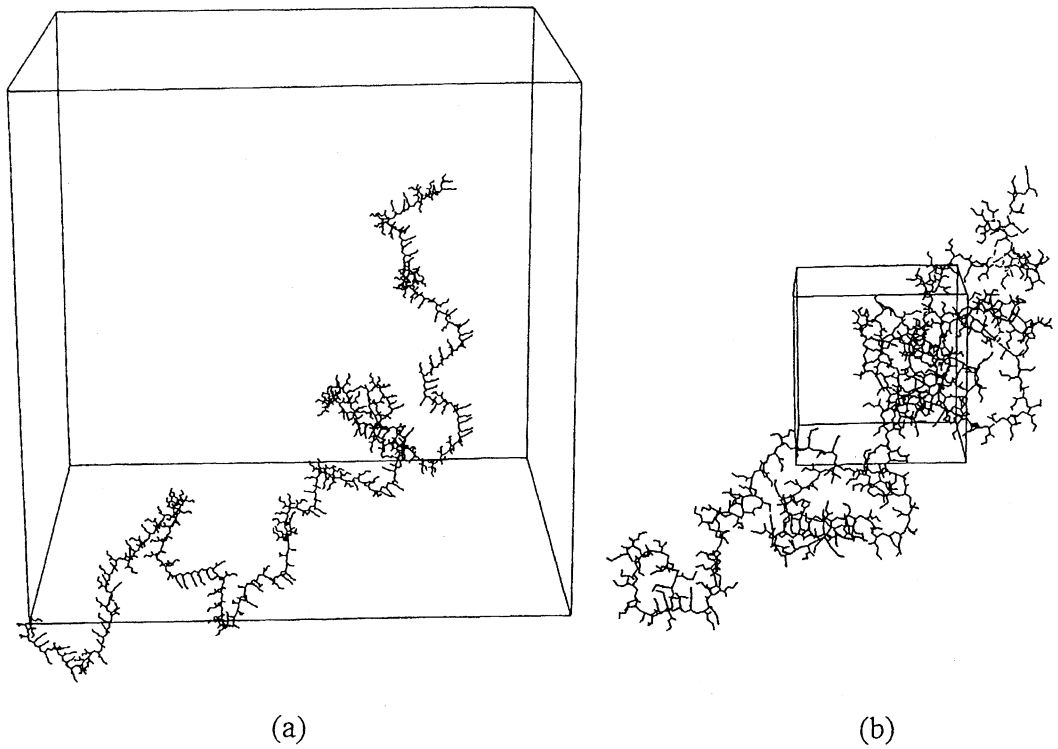

Fig. 2. PEA structures before and after the MD run: (a) the initial gas-like structure in which the cell-edge length is 184.4 Å and (b) the structure after 1.98 ns MD run, with the cell-edge lengths being 35.9 Å in average.

with the periodic boundary conditions. The gas-phase nature of the structure (a) is demonstrated by the large (cubic) cell with sides of 184.4 Å. In structure (b) the periodic cell has shrunk to a rectangular box of size $33.1 \times 37.7 \times 36.9$ Å^3. The polymer structure (b) is in a condensed phase as its periodic copies, which are not drawn in the figure, fill vacant spaces. The structure (b) has a density of 1.084 g cm^{-3}.

In general, stereochemical configurations of polymer chain have various rotational isomeric states (RIS) because of the steric hindrance. Therefore, we generated the polymer chain in Fig. 2(a) in a vacuum by using a RIS-type treatment. The elaborate Monte-Carlo chain-growth procedure of Theodorou and Suter[5)] was not performed. The RIS-type treatment we did was to generate a main-chain dihedral-angle sequence (more precisely, a RIS sequence) which contains only the dominant dyad conformations of vinyl polymers.[52)] The conformational composition of the dihedral-angle (RIS) sequence is given in Table 3. That is to say, we gave preferential dihedral angles to syndiotactic monomer pairs (*dl* and *ld*) and isotactic monomer pairs (*dd* and *ll*) along the polymer chain with the probabilities given in Table 3. The 3-dimensional structure constructed from the dihedral-angle sequence had a very high potential energy due to the occurrence of too short atom–atom distances. The high energy was released by applying an energy-minimization procedure, which produced the polymer chain in Fig. 2(a). The confor-

Table 3. Conformational Composition of PEA Structures[a)]

Conformation	Dyad tacticity[b)]			
	meso *dd*	*meso* *ll*	*racemic* *dl*	*racemic* *ld*
tt	0.000	0.000	0.976	0.976
	0.046	0.007	0.908	0.872
tg^-	0.000	0.563	0.000	0.000
	0.002	0.581	0.018	0.000
tg^+	0.516	0.000	0.000	0.000
	0.463	0.000	0.000	0.041
g^-t	0.484	0.000	0.000	0.000
	0.448	0.000	0.025	0.012
g^-g^-	0.000	0.000	0.024	0.000
	0.022	0.000	0.037	0.000
g^-g^+	0.000	0.000	0.000	0.000
	0.018	0.000	0.000	0.002
g^+t	0.000	0.437	0.000	0.000
	0.000	0.40	0.002	0.035
g^+g^-	0.000	0.000	0.000	0.000
	0.000	0.012	0.010	0.000
g^+g^+	0.000	0.000	0.000	0.024
	0.000	0.000	0.000	0.038

a) Results are shown for two structures. The upper entry is for the structure before the MD run. The lower entry is for the structures of the last 1 ns MD run (average). Each entry gives the ratio of a dyad conformation within a dyad tacticity. b) The symbols *d* and *l* refer to the asymmetric centers. The ratio of each dyad in the whole chain is: 0.207 for the *dd meso* dyad, 0.237 for the *ll meso* dyad, 0.278 for the *dl racemic* dyad, and 0.278 for the *ld racemic* dyad.

mational distribution of Table 3 did not change during the energy-minimization process.

The compression of structure (a) in Fig. 2 was done by applying a pressure of 100 atm during a MD run, at a temperature of 293 K. In order to prevent the periodic cell from shrinking too fast, the speed of the cell shrinkage was replaced by a limit value whenever the speed exceeded the limit. The limit value was a 0.01% change per step relative to the cell-edge length. The compression was continued for 80 ps (80000 steps) and the density was 1.04 $g\,cm^{-3}$ at the end. It is worth noting that the collapse of isolated polymer chains recently reported for polyethylene[53)] was not observed during the compression stage, as can be seen from a comparison of Figs. 2(a) and 2(b), where the global shape is mostly preserved.

After the compression process, the dynamics was run at 1 atm and 293 K for 1.9 ns of this last 1 ns was used to investigate molecular motions. The analysis is described in Ref. 1. The quantities not presented in Ref. 1 are discussed here. Table 3 compares the average conformational distribution with that of the initial structure. The small difference indicates that the change in the conformational structure is rather small during a total of 1.98 ns MD run. This observation is consistent with the notion of an extreme sluggishness of conformational relaxations in polymers.[17,18,54)] An expectation of a conformational relaxation beyond the reach of a practical MD run was the reason for the use of a RIS-type treatment in the chain-generation stage of the sample preparation.

Results and Discussion

Sample Quality: First of all, we focus our attention on the character of a sample prepared in a computer. MD results of the density and cohesive energy are compared with the experimental values[42—51)] in Table 2. The calculated density of PEA is in satisfactory agreement with the experiment value, though agreement is poor for the cohesive energy.

The quality of the computational PEA sample is fairly good, because its molecular motions are qualitatively or even semiquantitatively in agreement with the NMR experiments.[1)] The good agreement between the calculated and experimental densities also provides an added confirmation, especially because the force-fields were parametrized on small molecules. As for the cohesive energy, which requires further investigation, it must be noted that the cohesive energy is not a directly measurable quantity.[43)] In any case, further comparisons of MD results with experiments are desirable.[55)]

In order to obtain a good initial sample, condensation of the sample in the rubbery region is probably important, because it easily relaxes the system. The preparation procedure which we employed can not be used to make a glassy sample directly, while the method developed by Theodorou and Suter[5)] can be used. The procedure here, however, does not need any density data of the polymer. This point is significant because no polymer properties are needed to carry out a molecular dynamics simulation. To the best of our knowledge, there is no report that compares the method of Theodorou and Suter with the other sample preparation method in terms of sample quality.

One problem underlying some MD studies is whether the sample size is adequate to estimate polymer motion or not. Since the polymer sample which we employed consisted of one chain and its copies, the chain molecule is entangled with its copies. Our sample is therefore inadequate for quantitative analyses of the main chain dynamics accompanying large chain deformation i.e. reptation. However, the simulated sample has sufficient size to analyze side chain rotations, because the distance between a side chain and its copies is longer than 33 Å. It was noted that a similar degree of polymerization has also been employed in some recent research.[11,13,15,26)]

Glass Transition: Before discussing the molecular motions for polymers based on MD trajectories, it is necessary to determine whether the computational sample is glassy or rubbery at a given temperature. As described above, a computational PEA sample was prepared at 293 K. Using the structure after 1.9 ns MD run at 293 K as an initial structure, the specific volumes at a given temperature were generated by a cooling or heating procedure from the adjoining temperature. The MD runs at a given temperature were done for 1.3 ns each.

Figure 3 shows the temperature dependence of specific volumes averaged over the last 100-ps MD run. A break point regarded as a glass transition point was observed. The

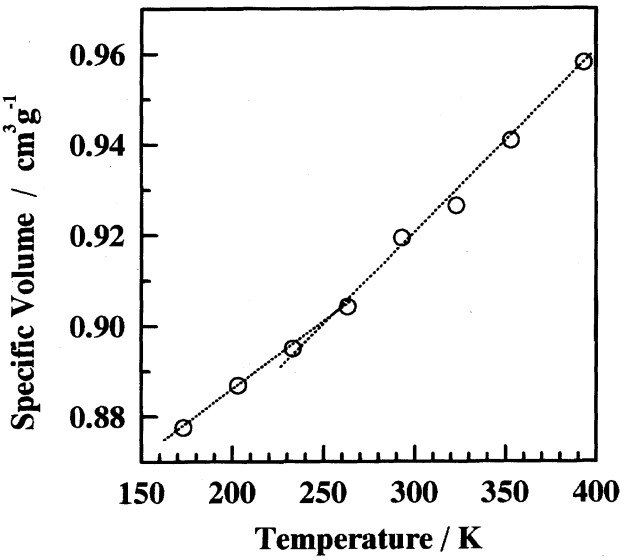

Fig. 3. Temperature dependence of specific volumes averaged over the last 100-ps MD run.

T_g value was 256 K, which is in agreement with the experimental T_g of 253 K. Han et al.[11] and Yamanaka[13] found that there is a tendency for the MD T_g values to be higher than the experimental ones. Yamanaka postulated that an upward temperature shift is due to the much higher rate of cooling when simulated as compared to the experimental conditions. The T_g value estimated from the MD trajectory is affected by the force-field parameters, simulation time and quality of the computational sample. To predict T_g by MD simulations, a more detailed study is required. Some investigators have already reported on the observation of the glass transition behavior using MD simulations.[9—13] These results are surprising in view of the fact that the experimental glass transition behavior is related to the relatively slower molecular motion. The reason why a glass transition can be observed in the MD simulation has not yet been clarified. In order to understand such a behavior, detailed investigations of the main chain dynamics are necessary.

The slopes for the data in Fig. 3 correspond to the thermal expansion coefficients. The estimated thermal expansion coefficients are 4.0×10^{-4} K^{-1} and 2.9×10^{-4} K^{-1} above and below T_g, respectively. The thermal expansion coefficient in the rubbery state obtained from the simulation was slightly smaller than the experimental value of 5.6×10^{-4} K^{-1}.[56] Unfortunately, the thermal expansion data of PEA was not found in the glassy region. Most of the thermal expansion coefficients for amorphous vinyl polymers in the glassy state are about 2.0—4.0×10^{-4} K^{-1}.[57—63] The thermal expansion coefficient in the glassy and rubbery state from the simulation was of the same order of magnitude as the experimental values for PEA or usual vinyl polymers. The agreement between the simulation and experiment is satisfactory.

Torsional Angle Autocorrelation Function: The molecular motions of polyacrylates were studied by combining solid state NMR relaxation experiments with molecular dynamics simulations.[1] It is difficult to analyze the inherent motion in the side chain using only NMR relaxation data, since the backbone motion superimposes on the side chain motions. MD simulations are suitable for analyzing such complicated motionsg. The inherent side chain motions are first extracted.

Autocorrelation functions are convenient for evaluating the local molecular motions. The torsional angle autocorrelation functions (TACF)[64] is defined as

$$\mathrm{TACF}(\tau) = <\cos\{\phi(t+\tau)-\phi(t)\}> = <\cos\{\Delta\phi\}>, \quad (1)$$

where $\phi(t)$ is the value of the torsional angle at time t, τ is an interval and the brackets denote ensemble averages. The decay rate of TACF is related to the only local mobility, which is not affected by surrounding motions.

Torsional Rotation around CH–C(carbonyl) Bond: The most interesting phenomenon is the torsional rotation of the side chain. Figure 4 shows the TACF for dihedral angles around the bond between methine carbons in the main chain and carbonyl carbons. A change in this angle involves the rotation of the entire side chain, since the end of the side chain is free. Obviously, the TACF strongly depends on the temperature. The TACF behavior reflects the distribution of the dihedral angle as well as the correlation time for rotational motions. In other words, the dumping rate of TACF corresponds to the frequency for rotational motions, while the asymptotic value at the infinite time depends on the distribution of the dihedral angle. Strictly speaking, the asymptotic value is a function of the distribution of $\Delta\phi$. Before discussing the molecular motions, it is necessary to be aware of the distribution of the dihedral angles at each temperature.

Figure 5 shows the distribution of the dihedral angles around the bond between the methine carbons in the main chain and the carbonyl carbons in the side chain at 203 and

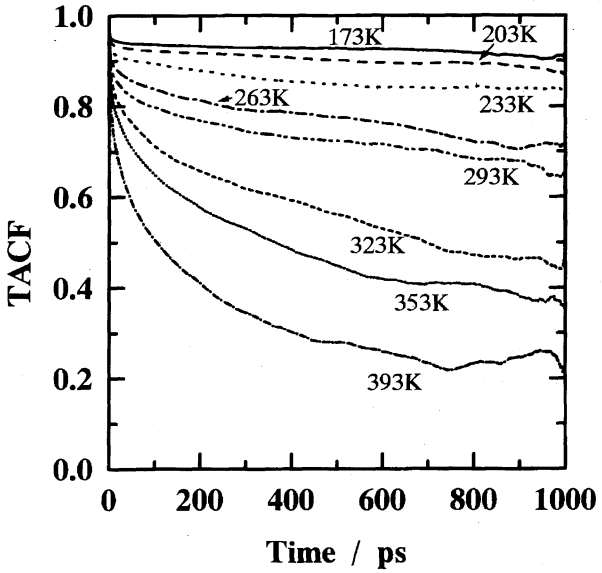

Fig. 4. TACF for dihedral angles of CH_2–CH–C(carbonyl)–O(non-carbonyl).

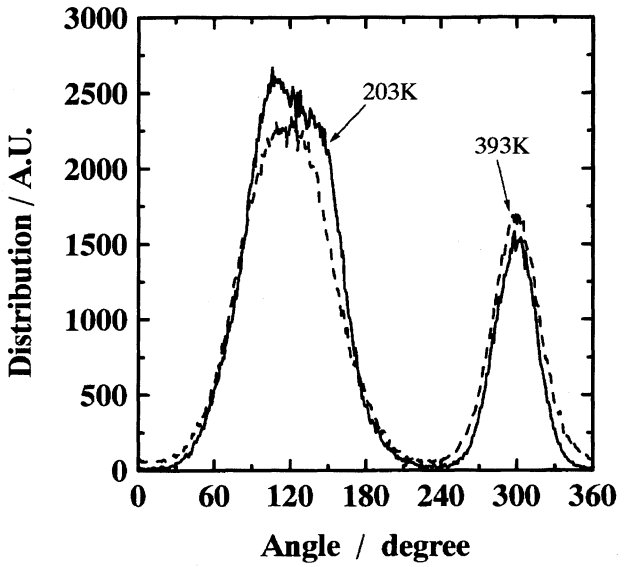

Fig. 5. Distribution of dihedral angles for CH_2–CH–C(carbonyl)–O(non-carbonyl) on the *d*-monomer unit at 203 and 393 K, where a dihedral angle of a trans conformation is defined as 180°.

393 K with respect to the *d*-monomer unit, where a dihedral angle of a *trans* conformation is defined as 180°. Although these distributions were classified by each triad sequence along the main chain, the distribution almost depends on the chirality of the center monomer unit. Now, we do not need to consider the distribution with respect to *l*-monomer unit because there is no physical difference between two enantiomers. Interestingly, two preferential conformations have different probability. This phenomenon can be understood as an effect of the asymmetric property of an ester group on the rotational angle distribution.

As shown in Fig. 4, all of TACF for the rotation of the entire side chain have initial rapid decay processes. The rapid decay is followed by a much slower loss of correlation. In order to determine the motional mode responsible for each decay process, typical trajectories of the torsional angle around the CH–C(carbonyl) for 1 ns duration at 393 K are plotted in Fig. 6. The rapid torsional oscillation corresponds to a rapid initial decay in TACF. In addition, occasional 180° conformational jumps are observed. The jump motion is obviously responsible for the dominant slower loss in TACF. This type of motion considerably decreases the TACF value, since $\cos\Delta\phi = -1$ in this case, where $\Delta\phi = 180°$. On the other hand, TACF drops to 0.95 at 203 K for several picoseconds, while the TACF slightly drops after an initial decay. Therefore, the dominant motion is rapid torsional oscillation rather than 180° jump motion in the low temperature region. It is concluded that the remarkable dumping of TACF at 393 K can be understood as the result of both the 180° jump motion and the increase in torsional oscillation with increasing temperature.

None of the TACF shown in Fig. 4 showed the characteristics of a simple exponential function. The superposition of two kinds motion and the anisotropic rotation of the side

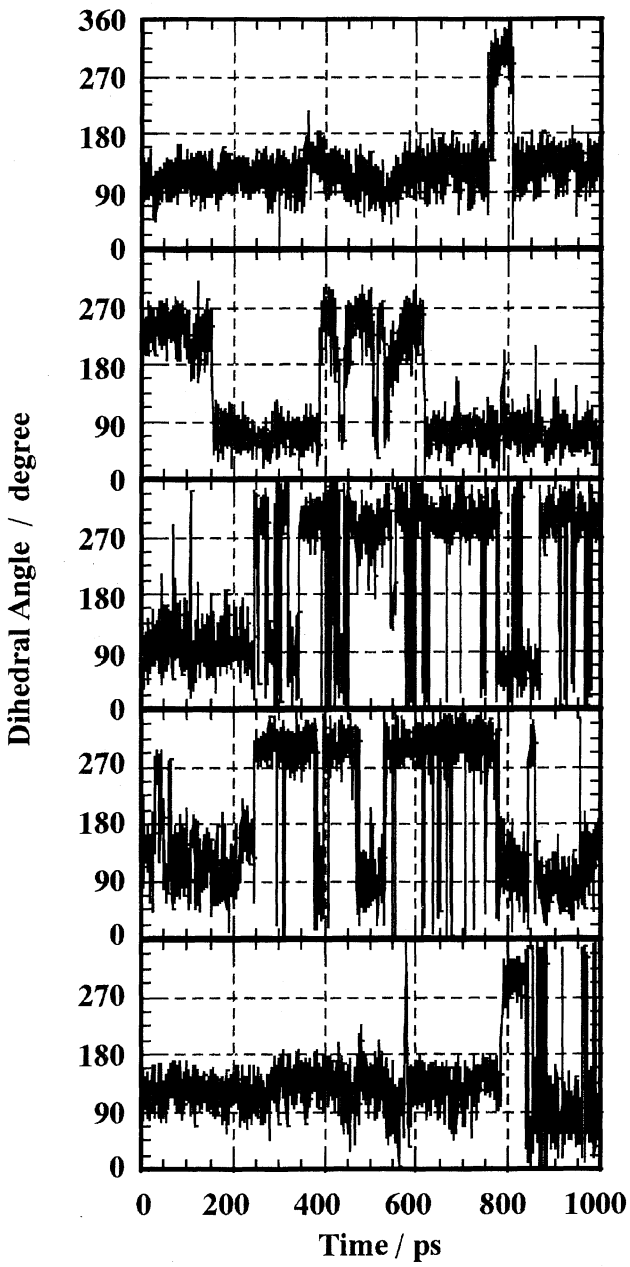

Fig. 6. Typical trajectories of five successive the dihedral angle for CH_2–CH–C(carbonyl)–O(non-carbonyl) for 1 ns duration at 393 K.

chain causes a deviation from a single exponential function. Extraction of the jump motion from MD trajectory is easy, and it is helpful for a quantitative analysis. The number of conformational jumps at each temperature was counted. We counted it for individual chirality because the preferential conformation depended on the chirality of the monomer unit. The conformational jump rate for torsional rotation around the CH–C(carbonyl) bond is plotted as a function of the inverse temperature in Fig. 7, where the jump rate is defined as the number of conformational jumps per bond per 1 ns. Ten conformational jumps were observed at room temperature. Assuming an Arrhenius relationship, we can estimate the activation energy of the conformational jump motion. The

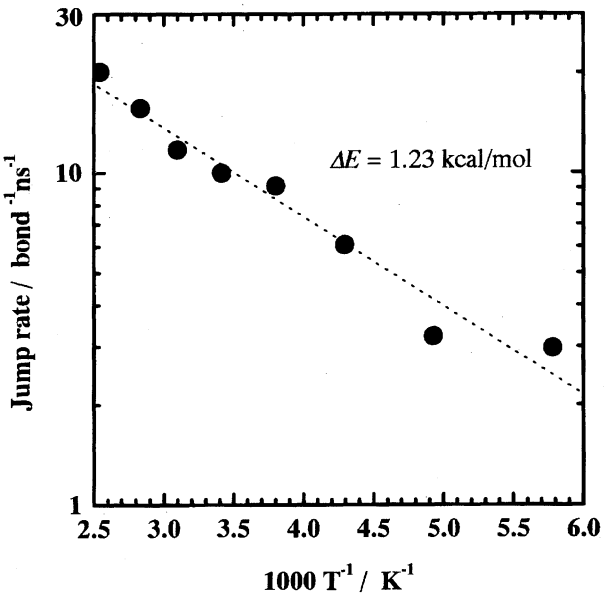

Fig. 7. Conformational jump rate for rotation of around the CH–C(carbonyl) bond as a function of inverse temperature, where the jump rate is defined as the number of jump motion per bond for 1 ns.

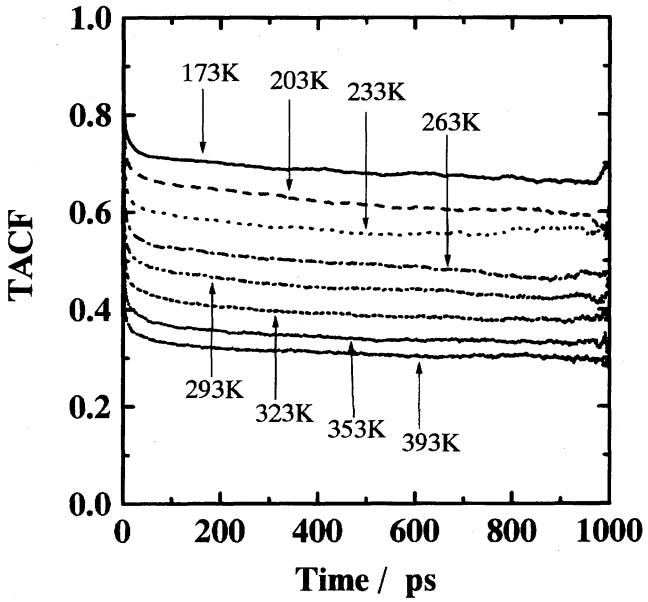

Fig. 8. TACF around the O(non-carbonyl)–CH_2 bond at each temperature for 1 ns.

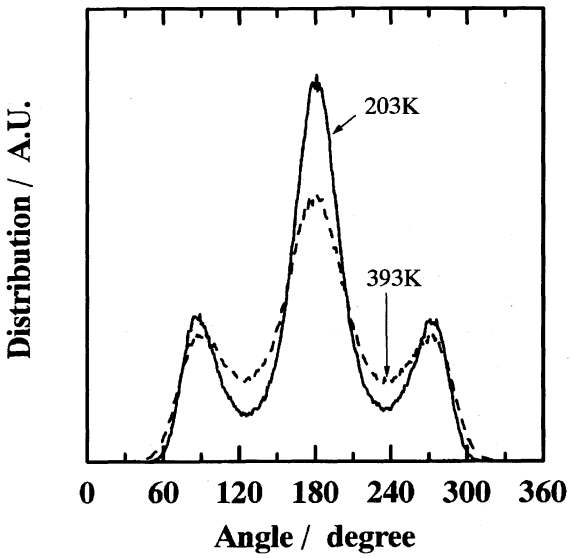

Fig. 9. Dihedral angle distribution for C(carbonyl)–O(non-carbonyl)–CH_2–CH_3 at 203 K (solid line) and 393 K (dashed line).

calculated activation energy was 1.23 kcal mol^{-1}.

It is interesting to compare the present results with the NMR relaxation data, because the observable correlation time from T_1 method partly agrees with that from MD simulations. Kawai investigated the dynamics of polyacrylates and polymethacrylates based on the spin-lattice relaxation time (T_1^H) measured over a wide temperature range.[30] According to Kawai, two relaxation processes are observed in PEA as T_1 minima, which correspond to the segmental motion and side chain motion. Kawai estimated the activation energy of the side chain relaxation process as $\Delta E = 1.9$ kcal mol^{-1}. The present result from MD simulations, $\Delta E = 1.23$ kcal mol^{-1}, did not agree with Kawai's result. The discrepancy is, however, reasonable, since T_1 data of the side chain actually includes both ethyl-group rotation and the entire side chain rotation. In addition, a single correlation time was assumed for the analysis of T_1 data despite the fact that the polymer dynamics is usually anisotropic. The activation energy calculated throughout the simulation was related only to the rotation around the CH–C(carbonyl) bond.

Ethyl Group Rotation: Figure 8 shows TACF around the bond between the non-carbonyl oxygen and methylene carbon in the side chain at each temperature. The feature of TACF around the O(non-carbonyl)–CH_2 bonds is considerably different from that of TACF around the CH–C(carbonyl) bonds. The initial drop in the TACF increased with increasing temperature. However, TACF decreased only slightly after the initial decay for the rest of the temperature range. In other words, only the asymptotic value of TACF varies. In order to find the motional mode, the distributions of the dihedral angle around the O(non-carbonyl)–CH_2 bond are shown in Fig. 9. There are three peaks at 90, 180, and 270°, which correspond to the preferential conformation of *gauche*$^-$, *trans*, and *gauche*$^+$, respectively. It should be noted that the central angles of the *gauche* conformation are 180±90° instead of 180±120°. Therefore, it was found that three-site jump motion occurred around the O(non-carbonyl)–CH_2 bond. In addition, it is interesting to note that the dihedral angles for the transition states between the *trans* and *gauche* conformation exist with considerable probability. The existence of a conformation at the transition state suggests that the energy gap between each conformation is approximately equal to the thermal energy in the temperature range under consideration. As the temperature increased, the boundary dividing *trans* and *gauche* conformations was obscured and the distribution broadened. Instead of a three-site

jump motion, the motional feature becomes a torsional oscillation with an angular distortion of ca. 240° in the higher temperature range. Another important fact is that there are no conformations near 0° of the dihedral angle. This indicates that the ethyl group motion is not a full 360° rotation, even at higher temperatures. This anisotropic rapid oscillation of the ethyl group caused an extremely high T_1^C minimum for the OCH_2 carbon in solid NMR relaxation experiments, which was reported in a previous paper.[1] The fact that TACF does not decrease after 10 ps can be interpreted to be due to anisotropic oscillation of several picoseconds.

In order to comprehend the temperature dependence of the ethyl group motion, the conformational jump rate were estimated by counting the number of jump motions. Figure 10 shows the conformational jump rate around the O(non-carbonyl)–CH_2 bond as a function of the inverse temperature, where the jump rate is defined as the number of jump motions per bond for 1 ns. The best fit to the logarithmic plot is demonstrated as the dashed line in Fig. 10. The slope gave an activation energy of 0.64 kcal mol^{-1}. The three-site jump rate around the O(non-carbonyl)–CH_2 bond at room temperature was ca. 500 $bond^{-1}$ ns^{-1} which corresponds to the occurrence of a single jump motion for 2 ps. This jump rate at room temperature is consistent with the result that the TACF fairly decays for 10 ps.

The effect of the inherent motion of the side chain on T_g is worth noting. The Arrhenius plots shown in Figs. 7 and 10 have no break point. This is because the activation energies neither for the 180° jump motion of entire side chain nor for the 3-site jump motion of ethyl-group change at T_g. It is worth emphasizing that the glass transition behavior is not directly affected by the inherent rotation on the side chain. Such a behavior is often observed by the ^{13}C spin-lattice relaxation time (T_1^C). Consequently, local side chain rotations can be regarded as being independent of the backbone motion.

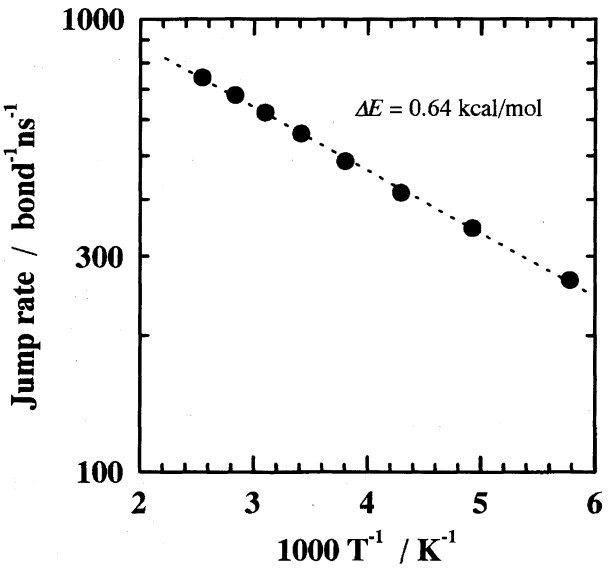

Fig. 10. Conformational jump rate around the O(non-carbonyl)–CH_2 bond as a function of inverse temperature, where the jump rate is defined as the number of jump motion per bond for 1 ns.

Conclusion

Atomistic molecular dynamics (MD) simulations have been carried out for a methyl-terminated atactic PEA using force-field parameters which we determined. The simulated density and T_g of PEA is in satisfactory agreement with the experiment. In order to analyze the local motion of PEA, TACF was calculated. Summarizing the side chain motion of PEA, it can be concluded that side chain motion involves 180° jump motion of the entire side chain with rapid torsional oscillation within stable conformations and three-site jump motion around the O(non-carbonyl)–CH_2 bond wrapped over a rapid torsional oscillation. The latter jump motion is two orders of magnitude faster than the former jump motion. Moreover, the activation energies for these jump motions above T_g were identical to those below T_g. This suggests that the inherent side chain motions are hardly affected by the main chain motion responsible for the glass transition.

In general, it is difficult to observe the side chain motion selectively in a laboratory system, because backbone motions superimpose on side chain motion. The advantage that some kinds of internal motion can be selectively observed by the MD simulation is quite attractive.

S. K. is grateful to Dr. H. Noma and Mr. T. Ohsaka for stimulating discussions.

References

1) H. Kikuchi, H. Tokumitsu, and K. Seki, *Macromolecules*, **26**, 7326 (1993).
2) M. S. Hedenqvist, R. Bharadwaj, and R. H. Boyd, *Macromolecules*, **31**, 1556 (1998).
3) M. Hutnik, F. T. Gentile, P. J. Ludovice, U. W. Suter, and A. S. Argon, *Macromolecules*, **24**, 5962 (1991).
4) D. Brown, J. H. R. Clarke, M. Okuda, and T. Yamazaki, *J. Chem. Phys.*, **100**, 1684 (1994).
5) D. N. Theodorou and U. W. Suter, *Macromolecules*, **18**, 1467 (1985).
6) D. N. Theodorou and U. W. Suter, *Macromolecules*, **19**, 139 (1986); **19**, 379 (1986).
7) R. H. Boyd and P. V. K. Pant, *Macromolecules*, **24**, 4073 (1991); **24**, 4078 (1991).
8) C. F. Fan and S. L. Hsu, *Macromolecules*, **25**, 266 (1992).
9) D. Rigby and R. J. Roe, *J. Chem. Phys*, **87**, 7285 (1987); **89**, 5280 (1988).
10) D. Rigby and R. J. Roe, *Macromolecules*, **22**, 2259 (1989); **23**, 5312 (1990).
11) J. Han, R. H. Gee, and R. H. Boyd, *Macromolecules*, **27**, 7781 (1994).
12) R. H. Boyd, R. H. Gee, J. Han, and Y. Jin, *J. Chem. Phys.*, **101**, 788 (1994).
13) H. Yamanaka and T. Koremoto, "Preprint of 8th Symposium on Molecular Simulation of Japan," Fukui Prefectural University, (Japanese) p. 86 (1994); "Preprint of 9th Symposium on Molecular Simulation of Japan," Keio University, (Japanese) p. 81 (1995).
14) H. Takeuchi, *J. Chem. Phys.*, **93**, 2062 (1990); **93**, 4490 (1990).

15) L. Fritz and D. Hofmann, *Polymer*, **38**, 1035 (1997).
16) A. A. Gray-Weale, R. H. Henchman, R. G. Gilbert, M. L. Greenfield, and D. N. Theodorou, *Macromolecules*, **30**, 7296 (1997).
17) F. Muller-Plathe, *J. Chem. Phys.*, **94**, 3192 (1991); **96**, 3200 (1992).
18) R. M. Sok, H. J. C. Berendsen, and W. F. van Gunsteren, *J. Chem. Phys.*, **96**, 4699 (1992).
19) K. Choi and W. H. Jo, *Macromolecules*, **28**, 8598 (1995).
20) H. Takeuchi, R. J. Roe, and J. E. Mark, *J. Chem. Phys.*, **93**, 9042 (1990).
21) K. F. Mansfield and D. N. Theodorou, *Macromolecules*, **23**, 4430 (1990); **24**, 4295 (1991); **24**, 6283 (1991).
22) L. Yang, D. J. Srolovitz, and A. F. Yee, *J. Chem. Phys.*, **107**, 4396 (1997).
23) D. Brown and J. H. R. Clarke, *Macromolecules*, **24**, 2075 (1991).
24) J. I. McKechnie, R. N. Haward, D. Brown, and J. H. R. Clarke, *Macromolecules*, **26**, 198 (1993).
25) C. F. Fan, T. Cagin, W. Shi, and K. A. Smith, *Macromol. Theor. Simul.*, **6**, 83 (1997).
26) N. E. Moe and M. D. Ediger, *Polymer*, **37**, 1787 (1996).
27) M. Hutnik, A. S. Argon, and U. W. Suter, *Macromolecules*, **24**, 5970 (1991).
28) G. D. Smith and R. H. Boyd, *Macromolecules*, **25**, 1326 (1992).
29) A. R. Tiller, *Macromolecules*, **25**, 4605 (1992).
30) T. Kawai, *J. Phys. Soc. Jpn.*, **16**, 1220 (1961).
31) J. L. Gomez Ribelles, J. M. Meseguer Duenas, and M. Monleon Pradas, *J. Appl. Polym. Sci.*, **38**, 1145 (1989).
32) B. Gabrys, J. S. Higgins, K. T. Ma, and J. E. Roots, *Macromolecules*, **17**, 561 (1984).
33) The program was written by S. Kuwajima mainly at CRC Research Institute, Inc., and partly elsewhere. The executable program was commercially available from CRC Research Institute, Inc. Now the modified program "NanoBox" is commercially available from Nano-simulation Associates.
34) S. Nose, *Mol. Phys.*, **52**, 255 (1984); *J. Chem. Phys.*, **81**, 511 (1984).
35) H. C. Andersen, *J. Chem. Phys.*, **72**, 2384 (1980).
36) M. Parrinello and A. Rahman, *Phys. Rev. Lett.*, **45**, 1196 (1980); *J. Appl. Phys.*, **52**, 7182 (1981).
37) If the relative hardness of the program coding is put aside, the Parrinello–Rahman (PR) type approach is best because it gives polymer samples full degrees of freedom to relax. However, more restrictive approaches like ours should work as well unless polymer samples are too small. In the MD studies of amorphous polymers the PR type approach is rather exceptional (e.g., Refs. 15 and 31).
38) H. J. C. Berendsen, J. P. M. Postma, W. F. van Gunsteren, A. DiNola, and J. R. Haak, *J. Chem. Phys.*, **81**, 3684 (1984).
39) D. E. Williams, *Acta Crystallogr., Sect. A*, **A27**, 452 (1971).
40) P. Linse and H. C. Andersen, *J. Chem. Phys.*, **85**, 3027 (1986).
41) W. L. Jorgensen, J. D. Madura, and C. J. Swenson, *J. Am. Chem. Soc.*, **106**, 6638 (1984).
42) G. Allen, G. Gee, D. Mangaraj, D. Sims, and G. J. Wilson, *Polymer*, **1**, 467 (1960).
43) D. Mangaraj, S. Patra, and S. Rashid, *Makromol. Chem.*, **65**, 39 (1963).
44) F. D. Rossini, K. S. Pitzer, P. L. Arnett, R. M. Brawn, and G. C. Pimentel, "Selected Values of Physical and Thermodynamic Properties of Hydrocarbons and Related Compounds," API Project 44, Carnegie Press, Pittsburgh, PA (1953).
45) R. C. Wackher, C. B. Linn, and A. V. Grosse, *Ind. Eng. Chem.*, **37**, 464 (1945).
46) R. de Mallemann, F. Suhner, and A. Malevergne, *Comptes Rendus*, **232**, 1385 (1951).
47) R. M. Kennedy, M. Sagenkahn, and J. G. Aston, *J. Am. Chem. Soc.*, **63**, 2267 (1941).
48) K. S. Howard and F. P. Pike, *J. Phys. Chem.*, **63**, 311 (1959).
49) R. E. Pennington and K. A. Kobe, *J. Am. Chem. Soc.*, **79**, 300 (1957).
50) S. A. Mumford and J. W. C. Phillips, *J. Chem. Soc.*, **1950**, 75.
51) V. Svoboda, V. Uchytilova, V. Majer, and J. Pick, *Collect. Czech. Chem. Commun.*, **45**, 3233 (1980).
52) P. J. Flory, "Statistical Mechanics of Chain Molecules," Interscience, New York (1969).
53) T. A. Kavassalis and P. R. Sundararajan, *Macromolecules*, **26**, 4144 (1993).
54) R. H. Boyd, *Macromolecules*, **22**, 2477 (1989).
55) Among the experiments which can be compared with MD results, the X-ray diffraction study will be the most important one with regard to the structure. On the other hand, global quantities such as the radius of gyration and end-to-end distance are unsuitable because these quantities do not equilibrate in the practical duration of the MD run (see Ref. 41).
56) P. Zoller and D. Walsh, "Standard Pressure-Volume-Temperature Data for Polymers," Technomic Publishing, Lancaster (1995), p. 171.
57) J. E. McKinney and M. Goldstein, *J. Res. Natl. Bur. Stand., Sect. A*, **78A**, 331 (1974).
58) C. K. Kim and D. R. Paul, *Polymer*, **33**, 2089 (1992).
59) S. S. Rogers and L. Mandelkern, *J. Phys. Chem.*, **61**, 985 (1957).
60) O. Olabisi and R. Simha, *Macromolecules*, **8**, 206 (1975).
61) P. Zoller and H. H. Hoehn, *J. Polym. Sci., Polym. Phys.*, **20**, 1385 (1982).
62) H. Shih and P. J.Flory, *Macromolecules*, **5**, 758 (1972).
63) T. Shiomi, F. Hamada, and T. Nasako, et al., *Macromolecules*, **23**, 229 (1990).
64) E. Kim and W. L. Mattice, *J. Chem. Phys.*, **101**, 6242 (1994).